3D geometries of normal faults in a brittle-ductile sedimentary cover: Analogue modelling

Lina Vasquez, Thierry Nalpas, Jean-François Ballard, Christian Le Carlier de Veslud, Brendan Simon, Olivier Dauteuil, Xavier D.U. Bernard

Accepted Manuscript

3D geometries of normal faults in a brittle-ductile sedimentary cover: Analogue modelling

Lina Vasquez, Thierry Nalpas, Jean-François Ballard, Christian LE Carlier DE Veslud, Brendan Simon, Olivier Dauteuil, Xavier D.U. Bernard

PII: S0191-8141(18)30206-2

DOI: 10.1016/j.jsg.2018.04.009

Reference: SG 3628

To appear in: *Journal of Structural Geology*

Received Date: 5 July 2017

Revised Date: 6 April 2018

Accepted Date: 10 April 2018

Please cite this article as: Vasquez, L., Nalpas, T., Ballard, Jean.-Franç., LE Carlier DE Veslud, C., Simon, B., Dauteuil, O., Bernard, X.D.U., 3D geometries of normal faults in a brittle-ductile sedimentary cover: Analogue modelling, *Journal of Structural Geology* (2018), doi: 10.1016/j.jsg.2018.04.009.

3D geometries of normal faults in a brittle-ductile sedimentary cover: Analogue modelling

Lina VASQUEZ[(1)], Thierry NALPAS[(1)], Jean-François BALLARD[(2)], Christian LE CARLIER DE VESLUD[(1)], Brendan SIMON[(1)], Olivier DAUTEUIL[(1)], Xavier DU BERNARD[(2)]

(1) University of Rennes, CNRS, Géosciences Rennes, UMR 6118, 35000 Rennes, France.

(2) Total SA, CSTJF, avenue Larribau, 64018 Pau cedex, France

Email: thierry.nalpas@univ-rennes1.fr

Abstract

It is well known that ductile layers play a major role in the style and location of deformation. However, at the scale of a single normal fault, the impact of rheological layering is poorly constrained and badly understood, and there is a lack of information regarding the influence of several décollement levels within a sedimentary cover on the single fault geometry under purely extensive deformation. We present small-scale experiments that were built with interbedded layers of brittle and ductile materials and with minimum initial constraints (only a velocity discontinuity at the base of the experiment) on the normal fault geometry in order to investigate the influence of controlled parameters such as extension velocity, rate of extension, ductile thickness and varying stratigraphy on the 3D fault geometry. These experiments showed a broad-spectrum of tectonic features such as grabens, ramp-flat-ramp normal faults and reverse faults. Forced folds are associated with fault flats that develop in the décollement levels (refraction of the fault angle). One of the key points is that the normal fault geometry displays large variations in both direction and dip, despite the imposed homogeneous extension. This result is exclusively related to the presence

of décollement levels, and is not associated with any global/regional variation in extension direction and/or inversion.

Keywords: analogue modelling; décollement level; extensional forced fold; ramp-flat-ramp normal faults

1. Introduction

In extensional basins, the deformation style is largely influenced by the rheology of the different deposits filling it. This is well-known in large-scale objects such as the lithosphere (e.g. Davy et al., 1995; Dauteuil et al., 2002), or even at a smaller scale such as the interaction between a sediment cover and basement faults (Vendeville, 1987; Withjack et al., 1990; Stewart et al., 1996; Hardy and McClay, 1999; Withjack and Callaway, 2000; Richardson et al., 2005; Fossen and Rotevatn, 2016). However, at the scale of a single fault, the impact of rheological layering is poorly constrained and poorly understood; only layer rotation around vertical fault overlap zones (Rykkelid and Fossen, 2002), or small-scale relay zones between normal faults (Kristensen et al., 2008) have been considered. Field examples show the influence of a layered system on the pattern of faults with a flat-ramp fault geometry at both the thin-section scale (Fig. 1a) and outcrop scale (Fig. 1b). Few seismic examples associate small zones of flat normal fault geometry with the presence of salt (Fig. 1c). In general, normal faults associated with a décollement level present a decrease in dip at depth, with development of a wide flat, and are considered as listric faults. This typical geometry is identified and studied at the seismic scale (Fig. 1d), and reproduced through sandbox modelling (Fig. 1e). Previous works, especially using analogue modelling, have investigated the impact of a pre-cut flat-ramp fault geometry on deformation (McClay and Scott, 1991; McClay, 1990) as well as the effect of a single décollement layer at the base of the experiments (Higgins and Harris, 1997;

Withjack and Callaway, 2000; Withjack et al., 1990). This analogue modelling did not investigate the initiation of the flat geometry of the normal fault during extension.

The aim of this paper is to study the geometry of normal faults at a local scale, created in pure extension context, when cutting potential décollement layers. It is critical to know how to identify reverse faults or folds created during pure extensional deformation as observed in the field (Sharp et al., 2000) or analogue modelling (Horsfield, 1977; Vendeville, 1987; Withjack et al., 1990; Ge and Jackson, 1998; Withjack and Callaway, 2000; Dooley et al., 2003; Soto et al., 2007) in order to avoid interpreting these structures as related to inversion or strike-slip movement.

Here, we present a series of small-scale physical experiments that were built with interbedded layers of brittle and ductile materials and without any initial constraints on the normal fault geometry. In addition, the fault geometries observed at the final stage of deformation are only related to the rheology of the layers. We used analogue modelling to study the impact of several ductile layers on deformation (geometry of the layers and faults) as well as mechanical parameters: rate and amount of extension, ductile thickness, and varying stratigraphy (Table 1) followed by a 3D geometrical model built from the results of one of our experiments (experiment 3). Our results show that the specific pattern of normal faults with a ramp-flat-ramp geometry of the associated reverse faults are only related to pure extension and not associated with any global/regional variation in extension direction and/or inversion.

2. Experimental protocol

2.1. Analogue materials

In this study, we used the classical techniques of analogue modelling applied for brittle/ductile experiments developed by the Experimental Tectonics Laboratory of Géosciences Rennes

(Université de Rennes 1, France). These techniques have been described in various previous works dealing with the use of a velocity discontinuity (VD; e.g. Malavieille, 1984; Balé, 1986; Ballard et al., 1987; Allemand et al., 1989), the use of silicone and sand as analogue materials (Faugère and Brun, 1984), as well as various scaling issues (Davy and Cobbold, 1991; Weijermars et al., 1993). In order to simulate the brittle behaviour of sedimentary rocks with Mohr-Coulomb properties, two materials were used: (i) dry Fontainebleau quartz sand (manufactured by SIBELCO France), with a mean grain size of approximately 250 μm, an internal friction angle of 30-35° (Krantz, 1991) and a volumetric mass density (ρ) of approximately 1500 kg/m^3, (ii) microbeads (manufactured by CVP France) with a lower internal friction angle than sand of 20-22° and a volumetric mass density (ρ) of approximately 1480 kg/m^3 (Panien et al., 2006).

Silicone putty was used to simulate the ductile behaviour of viscous sedimentary rocks such as evaporite, or under compacted and over-pressured shale (e.g. Cohen and McClay, 1996; Wu and McClay, 2011). Given that weak sedimentary rocks have different strengths in nature, we used two silicone putties in order to represent décollement levels with different strengths in the same experiment. The strongest silicone is a pink silicone putty with a mean viscosity close to 6 10^4 Pa.s at 20°C and a mean volumetric mass density of approximately 1300 kg/m^3 (Rhodorsil Gomme GS1 RG 70 009 manufactured by Rhône-Poulenc, France). The weakest silicone is a transparent silicone putty with a mean viscosity close to 3 10^4 Pa.s at 20°C and a mean volumetric mass density of approximately 970 kg/m^3 (silicone putty SGM 36, manufactured by Rhône-Poulenc, France).

2.2. Experimental apparatus

The experimental apparatus consists of a fixed wall screwed to a rigid and fixed basal plate, over which another wall is fixed to a thin mobile basal plate (Fig. 2). The mobile basal plate and wall are pulled at a constant rate perpendicularly to the wall. A 5 cm wide sand wall supports the two other sides; the first centimetres of the experiment near these sand walls, where there are significant

96 border effects, are not considered. The displacement of the basal mobile plate induces a velocity
97 discontinuity (VD), which localises the deformation at the base of the experiment in the middle of
98 the experiment (cf. Malavielle, 1984; Balé, 1986; Ballard, 1989). The experiment is set up in a 40
99 cm wide and 60 cm long apparatus with a 12.5 cm thick stratigraphy (Fig. 2, Table 1) that is wide
100 enough to allow the experiment to be cut into several vertical slices and studied outside the zone of
101 the border effects.

102 From base to top, the reference stratigraphy of the experiments (e.g. experiment 3) was made up of
103 (Fig. 2 and 3):
104 - 1 cm of light brown silicone layer, a rectangular band measuring approximately 5 cm wide,
105 located all along the VD (basal silicone);
106 - 3.5 cm (2.5 cm above the basal silicone) of black and white coloured sand (sand 1);
107 - 0.5 cm of white microbeads (microbeads);
108 - 2.5 cm of black and white coloured sand (sand 2);
109 - 0.5 cm of pink silicone putty (lower Silicone);
110 - 2.5 cm of black and white coloured sand (sand 3);
111 - 0.5 cm of transparent silicone putty (upper Silicone), and
112 - 2.5 cm of black and white coloured sand (sand 4). Black sand was sprinkled in very thin layers at
113 the top of the experiment.
114 The basal silicone is located above the VD in order to distribute the deformation and generate a
115 larger zone of deformation with the clearly separated normal fault. The sand layers represent brittle
116 pre-kinematic formations with Mohr-Coulomb behaviour. The lower and upper silicone layers
117 represent potential décollement layers with ductile behaviour, while microbeads represent a level
118 with Mohr-Coulomb behaviour with a lower internal friction angle than sand. Part of the sand was
119 coloured black in order to construct the experiment in layers and to make it easier to observe the

deformation in the cross-sections; the colouration does not influence the mechanical properties of the sand.

This reference stratigraphy was used for most of the experiments (experiments 1 to 8). In order to analyse the effect of the thickness of the ductile layers, we tested an experiment (experiment 9) with half the thickness of the ductile layers. In order to test the stratigraphic organisation of the ductile layers, we inverted the upper transparent silicone with white microbeads in one experiment (experiment 10).

This mechanical layering can be used to vary the mechanical behaviours in a heterogeneous system through a saw tooth strength profile (Fig. 2), thereby causing a broad variability in normal fault geometries.

2.3. Experimental deformation process

In the first set of experiments, the deformation was achieved by pulling the mobile basal plate perpendicularly to the VD at a defined and constant velocity (ranging from 0.25 cm/h to 4 cm/h) in order to generate 1 cm of pure extension.

In the second set of experiments, the deformation was achieved by pulling the mobile basal plate perpendicularly to the VD at a defined and constant velocity of 1 cm/h (like reference experiment 3), but with a varying amount of displacement (ranging from 0.5 cm to 4 cm).

In the third set of experiments, the deformation was achieved by pulling the mobile basal plate perpendicularly to the VD at a defined and constant velocity of 1 cm/h (like reference experiment 3), but with a variation in the stratigraphic setup of the ductile layers.

Photographs of the top surface of the experiment were taken every 1 mm of extension. At the end of the experiment, white sand was sprinkled in a thick layer to preserve the surface deformation of the experiment surface, and then humidification was performed in order to cut the experiment

perpendicular to the VD. The cross-sections were made every 2 cm through the central part of the experiments giving twelve sections. The photographs of the cross-sections record the final deformation state throughout the experiments highlighted by the colours of the layers.

3. Experimental results

3.1. General features

The main structural features encountered in most of the experiments are two major normal faults connected at depth to the borders of the basal silicone sheet (Fig. 3). These faults may or may not show a flat within the lower and upper silicone layers (Fig. 3). Flats in the upper transparent silicone layer are wider and more common than in the pink lower silicone layer. Associated with the flat, the ductile layers are thinned as a consequence of pure shear deformation that accommodates extension in the ductile layer. Above the flat, the sand layers may display a continuous deformation represented by an accommodation extensional fold (e.g. Schlische, 1995; Withjack and Callaway, 2000; also see Cosgrove and Ameen, 2000 and references therein) (Fig.3b). Above the flat, the sand layers also display a graben above the silicone layer as observed previously in analogue modelling (e.g. Vendeville, 1987; Nalpas et al., 1995; Brun and Nalpas, 1996; Withjack and Callaway, 2000; Dooley et al., 2003). The major border normal fault, affecting the upper sand layer, may also evolve as a reverse fault upward.

Between the two major normal faults, minor normal faults affect the brittle layers under the lower silicone layer and cut the microbeads without creation of a flat.

3.2. Influence of extension rate

Five cross-sections from different experiments (experiments 1 to 5; Table 1) with the same standard layering illustrate the influence of extension rate (from 0.25 to 4 cm/h) and consequently mechanical behaviour in the ductile layers of the final deformation after 1 cm of extension (Fig. 4).

For the highest extension rate (4 cm/h - Fig. 4a, experiment 5), two normal faults affect the whole experiment with the major one located on the left side. No observable flat is present associated with either the lower silicone layer or reverse fault. A graben, associated with a flat, accommodates the flexural deformation of the upper sand layer on the right side of the experiment above the upper silicone layer. Several normal faults affect the lower sand layers and microbeads below the lower silicone layer.

For intermediate rates of 1 or 2 cm/h (Fig. 4b and c, experiments 3 and 4, respectively), two major faults are refracted in the silicone layer, and develop a ramp and flat geometry when crossing silicone layers. This ramp-flat-ramp geometry may evolve in two ways: either as a fault lens (Fig. 4b zoom) or as a flat with an extensional forced incipient fold (Fig. 4c zoom). In the case of a fault lens (Fig. 4b zoom), the sand layers (sand 3) are deformed by translation along the faults without rotation. In the case of a flat (Fig. 4c zoom), the sand layers (sand 3) are deformed by flexure, with creation of an extensional forced fold, affecting the hanging wall only above the flat. Note that this incipient fold, created only in extension, corresponds to an anticline fold in the hanging wall of the normal fault, while drag folds (more hanging-wall synclines) develop generally along normal faults when there is no flat.

For the lowest rate of 0.5 and intermediate rates of 1 or 2 cm/h (Fig. 4b, c and d, experiments 2, 3 and 4 respectively), the major faults (red bold line in figures) evolve near the surface in the sand layers (sand 4) from a normal fault to a reverse fault (Fig. 4d zoom).

For the lowest rates of 0.25 or 0.5 cm/h (Fig. 4d and e, experiments 1 and 2, respectively), only one major fault cuts the whole stratigraphic pile that concentrates the deformation and one or two

antithetic normal faults below the lower silicone layer. With a very low velocity of extension 0.25 cm/h (Fig. 4e, experiment 1), only one antithetic normal fault is located near the major normal fault, which produces a narrow deformed zone, and the associated subsidence above the lower silicone layer is accommodated by a flexural deformation of the sand layers. The ramp-flat-ramp fault geometry is emphasised for a very a low velocity (0.25 cm/h, Fig. 4e zoom). The global deformation of the sand layers in the hanging wall between the two silicone layers corresponds to a faulted evolved extensional forced anticline fold. Note that the flats are best developed in the last experiment with a very low rate of extension.

Even though the extension direction is the same for all experiments, note that the major normal fault is sometimes located on the right side (experiments 1, 3 and 5) and sometimes on the left side (experiments 2 and 4). That means that the basal silicone layer decreases the initial constraints created by the velocity discontinuity situated at the base of the experiment. Similarly, the fault geometry and associated deformation are neither symmetric nor cylindrical, as can be seen on the top view of the final state of experiment 3 (Fig. 3). The left side of the experiment shows numerous closely spaced normal faults and a curved reverse fault. The right side of the experiment shows not straight normal faults that resemble an “en échelon” pattern. Note that the reverse fault and "en échelon" fault created here both result from pure extension.

3.3. Non-homogeneous geometries illustrated by the 3D model of experiment 3

As suggested by Figure 3, even though the applied displacement and the building of the experiment are homogeneous, the final deformation is neither symmetric nor cylindrical. Thus, in order to further investigate the lateral variations of both fault shapes and layer geometries, a 3D model was built using the gOcad modeller (Mallet, 2002) from twelve cross-sections of experiment 3 (Fig. 5).

The model building comprises two steps:

- The integration of the 3D cross-section data and the correlation of the cross-sections amongst themselves (coherency must be checked). The cross-sections are then used as a base to model faults and horizons.

- The construction of the 3D structural model with faults and horizons following geological and geometrical coherency rules (Caumon et al., 2009). This construction is made from the twelve cross-sections of experiment 3 (see example in Le Carlier de Veslud et al., 2009) using the DSI interpolator (Discrete Smooth Interpolation, Mallet, 2002). Faults are built first, followed by the layers that are then made to be consistent with the faults according to their continuous versus faulted behaviour as seen in the cross-sections.

As previously mentioned, décollement levels within the system lead to a broad diversity in the extensional structures related to the normal faults. The 3D numerical model enables a better visualisation and understanding of these non-homogeneous geometries (Fig. 5):

- The geometry of the fault planes corresponds to an undulating surface.

- Fault surfaces are not necessarily continuous and are organised "en échelon".

- The flat parts of the normal faults are not continuous and vary laterally in width, but are systematically associated with décollement levels.

- Some faults present normal dip at depth and turn to reverse faults upwards.

It is not straightforward to obtain information from the top view (Fig. 3) where only fault traces are visible in the 3D fault network (Fig. 5). This example demonstrates that, in a multi-layered system with several décollement levels, surface data with one cross-section are simply not sufficient enough to thoroughly reconstruct the fault network in depth as the deformation is complex.

Moreover, a partial observation can be misleading since the faults on the right-hand side of Figure 5 show an "en échelon" pattern that could suggest strike-slip movements whereas none are involved in our experiments at all.

3.4. Influence of the extension amount

Four cross-sections coming from four different experiments (experiments 3, 6, 7 and 8) carried out with the same standard stratigraphy and the same rate of extension of 1 cm/h illustrate the influence of the amount of extension from 0.5 to 4 cm (Fig. 6).

For an extension amount of 0.5 cm (Fig. 6a, experiment 6), the faults clearly cut the base layer of the experiment (sand 1, microbeads and sand 2) and are incipient in the middle part (sand 3); no faults affect the upper part of the experiment (sand 4). No variation in fault dip is observed. Flats are observed in the lower pink silicone, mainly on the right side of the cross-section. The deformation of the upper part of the experiment corresponds to a zone of subsidence limited by flexures situated above the two faults affecting the middle part of the experiment.

For an extension of 1 cm (Fig. 6b, experiment 3), which corresponds to the reference experiment with a standard stratigraphy as described previously (Fig. 4c), we observed the main characteristics with the creation of a graben, a normal fault to a reverse fault, and flat and fold related to the interaction between the sand and silicone layers during the extension. Note that the deformation affects all layers, with well-developed flats in the silicone layers.

For an extension of 2 cm (Fig. 6c, experiment 7), like FANEX 4, two major faults are developed with a ramp and flat shape when they cross the silicone layers. This ramp-flat-ramp geometry may evolve in two ways: either as a fault lens (Fig. 4b, right side) or as an overlap fault (Fig. 6c zoom). Above this overlap, the forced fold, affecting the hanging wall of the fault is partially faulted on its left side by a steep fault. The major fault evolves near the surface with an increase in the deformation of the upper sand layers (sand 4), with a graben on the platform border and a reverse fault in the direction of the subsidence zone. In the centre of the experiment between the two major normal faults, minor normal faults not only affect the brittle layers under the lower pink silicone layer but also the sand layer under the upper transparent silicone layer.

For an extension of 4 cm (Fig. 6d, experiment 8), the location of the structures is similar to the previous experiment, but the geometry is more complex, and the displacements and number of faults increase. In particular, the sand layers between the two silicone layers on the right side of the graben are deformed in the footwall of the normal fault associated with the gliding of the upper sand layer into the graben.

Note that, between the two normal faults created in the upper sand layers of the experiments, the subsidence zone is more developed (wider) when the upper sand over the transparent silicone is gliding in the direction of the central graben.

3.5. Influence of the stratigraphy of the décollement layers

Three cross-sections from three different experiments (experiments 3, 9 and 10) illustrate the influence of the mechanical layering (Fig. 7). Experiment 9 is built according to the same standard stratigraphy but the thicknesses of the silicone layers are roughly divided by two in experiment 9 (see Table 1). In experiment 10, the transparent upper silicone layer is swapped with the microbeads layer compared to experiment 3 (see Table 1).

When the silicone layers are thinner than in the reference layering (Fig. 7a, experiment 9), the faults tend to cross the whole experiment straight forward, without dip variation. Only a fault lens develops on the right side of the experiment between the lower and upper silicone layers. No grabens, reverse faults, flats, with an associated fold, or flexures are observed in this experiment. Note that the geometry of the structures is close to the experiment with a high extension rate (Fig. 4a, experiment 5).

When the silicone layers are in a reversed order (Fig. 7c, experiment 10), two normal faults, a major one (right side) and a minor one (left side), are developed in the upper sand layers of the experiments. The flat in the transparent silicone is wider than in experiment 3 and is associated with grabens between the silicone layers. As for experiment 9, no reverse faults are developed.

Note that, between the two normal faults created in the upper sand layers of the experiments, a subsidence zone develops and the width of this zone increases from experiment 9 to 10. In experiment 10, the major flats are developed in transparent silicone, which is located near the base of the experiment, resulting in a wider subsidence zone in the top; therefore, the deeper the flat, the wider the subsidence zone.

4. Discussion

4.1. Mechanical layering effect

The integration of a layer of microbeads, with a low internal friction angle, does not influence the geometry of the normal faults and their dip and therefore does not act as a décollement level (Fig. 8). In extensional experiments, it seems necessary to associate a slope of the layers with fluid overpressure during extension to produce a flat fault in the microbeads (Lacoste et al., 2012). The effects of fluid overpressures and slope in the sand experiments have also been previously suggested to induce gravitational gliding (Mourgues and Cobbold, 2003). Thus in our modelling, the most important mechanical layers are the viscous layers, the location of which largely drives the deformation pattern (Fig. 8).

The development of the flats is related to the strength ratio between the sand and silicone layers; the higher the strength ratio, the wider the flats.

In experiment 3 (Fig. 4), the flats are more developed in the transparent silicone than in the pink silicone, because the transparent silicone is two times less viscous than the pink silicone, and therefore the strength ratio between the sand layer and silicone layers is larger. This is consistent with our observations related to a velocity effect where the flat is larger when the strain rate is lower.

In experiment 9 (Fig. 7), where the thicknesses of the lower and upper silicone layers are roughly divided by two, compared to experiment 3 (0.5 cm in experiment 3 and 0.25 cm in experiment 9, see Table 1), the flats are nearly inexistent due to the decrease in the strength ratio.

In experiment 10 (Fig. 7), where the upper transparent silicone layer replaces the microbeads layer, compared to experiment 3, the flats are more developed in the transparent silicone located deeper in the experiment because the strength ratio is much higher. Note that the amplification of the flat length at depth in the experiment induces an increase in the width of the zone of subsidence without an increase in the amount of extension (Fig. 7c).

4.2. Strain rate effect

The strain rate controls the strength of the viscous layer (silicone): the higher the rate, the higher the strength; therefore, variations in the strain rate may impact the fault pattern, particularly in terms of the number of faults and their organisation. When the strain rate is greater than or equal to 1 cm/h (Fig. 4a, b and c), two main faults develop from the basal silicone and cut the whole experiment on the right and left side. When the strain rate is less than 1 cm/h (Fig. 4d and e), only one main fault develops from the basal silicone and cuts the whole experiment on the right or left side. This means that when the strain rate is high, the global deformation is more distributed and controlled by the strength of the silicone layers whereas when the strain rate is low, the global deformation is more localised and controlled by the strength of the sand layers (e.g. Davy et al., 1995). When the strain rate is low (Fig. 4e), the strength of the silicone layers decreases and the silicone layers act more as a décollement level and the deformation of the sand layers is only concentrated in one major fault or deformation zone (localisation of the deformation in the brittle layers).

The second effect, related to the first one, is the increase in flat size, mainly in the experiment with the lowest strain rate (0.25 cm/h). The increase in flat size is consistent with the decrease in silicone strength associated with the low strain rate, which supports efficient décollement levels. The

creation of flats induces specific deformation of the layers in the hanging wall with the development of forced folds (e.g. Jackson and Rotevatn, 2013; Lewis et al., 2013) or reverse faults at the top of some experiments. The characteristic features of both folds and reverse faults result from pure extension and are not indicative of a strike-slip component, compression or inversion interpretation.

These forced folds are parallel to the border fault and only located in the hanging wall above a flat without any "en echelon" character. They result from differential subsidence in the hanging wall: along the normal fault and within the graben, the subsidence of the sand layers is larger than above the flat where the subsidence of the sand layers is lower (see the red arrows in Fig. 8). These forced folds correspond to the seismic example given in Figure 1c (Jackson and Rotevatn, 2013). In the cross-section, just above and below the folded layers, the layers are flat, which means that compression or inversion cannot be used to explain the geometry of these layers. Moreover, it is possible to generate shortening in a pure extensive context, related to a local layer reorganisation between faults, for example in a system where the layers cannot move laterally. Similarly, "en échelon" structures can be observed locally, as in Figure 5, just in order to accommodate a local organisation of the deformation of the layers, without this making sense on a global scale.

4.3. Effect of the amount of extension

The first effect on the fault pattern is the number of faults generated inside the experiment. When the extension amount increases (Fig. 6), the two border main faults become more and more complex upward, in particular with a gliding amplification of the upper sand layer (sand 4) towards the graben (Nalpas and Brun, 1993). At the same time, the genesis of secondary conjugate normal faults between the two major border faults, in the centre part of the graben, produces a complex deformation of the lower and middle sand layers (sand 1, 2 and 3). In contrast, in the centre of the graben, the upper sand layer (sand 4) accommodates the deformation only by homogeneous subsidence. This is related to the decoupling between sand 4 and the lower layers allowed by the

upper silicone layer. As a result, the increase in the amount of extension is distributed along more faults, in the centre of the graben in lower layers and on the borders of the graben in upper layers.

The second effect is related to the flat genesis: the size of the flats located in the lower and upper silicone layers are not the same. For the lower silicone layer, the flat is not conserved during extension and an overlap, between normal faults affecting sand 2 and sand 3, is created in relation to the huge vertical throw of the fault (Fig. 6c). For the upper silicone layer, the subsidence between the two major faults, affecting the sand 1, 2 and 3 layers, induces a wide flat that results in the layers of sand 4 gliding above the upper silicone layer (see also Nalpas et al., 1993; Withjack and Callaway, 2000). This wide flat increases the zone of subsidence related to extension (Fig. 6a to d).

The third effect is both the creation and amplification of the movement of the upper reverse faults, affecting sand 4, associated with differential subsidence (Fig. 6). These faults have been previously described in analogue modelling (e.g. Horsfield, 1977; Vendeville, 1987; Withjack et al., 1990; Ge and Jackson, 1998; Dooley et al., 2003; Soto et al., 2007). In general, they are restricted to the upper sand layers, but they potentially develop inside the experiment between two layers of silicone (see sand 3 in Fig. 4e). They are related to the gliding and rotation of the sand layer in the direction of the graben resulting from the variation in subsidence velocity between the graben and its platform borders (Fig. 8). These reverse faults are systematically branched at depth on a décollement level, and are observed for the experiments with a variation in both the amount and rate of extension (Fig. 4). This structure corresponds to local deformation and does not provide any information about the boundary conditions. Thus, it is very important to recognise that these reverse faults may be generated in a pure extensional system, and to not associate them systematically with compression, strike-slip movement or inversion.

5. Conclusions

The presence of a décollement level largely controls the geometry of normal faults characterised by distinctive associated structures such as ramp-flat-ramps, forced folds and reverse faults all developing in a pure extension context.

- The genesis of flats along normal faults depends on the strength ratio between the sand and silicone layers: the higher the strength ratio, the wider the flats. Thus, the lower the velocity of the extension, the thicker the décollement layer, or the deeper the location of the décollement layer, and the wider the flat.

- A forced fold, associated with the flats, develops in the hanging wall and is characteristic of the presence of a décollement level as well as a flat just under the fold. Therefore in seismic interpretations, the presence of forced folds may be a good proxy to locate the décollement levels in sedimentary series and potential associated permeability barriers.

- Gliding reverse faults develop in the hanging wall on the border of the normal faults of the graben. They result from a variation in the subsidence velocity and accommodate the differential subsidence in the sand layers near the border of the normal fault of the graben. They are not related to shortening but are typical structures created in extension and are facilitated by the presence of a décollement level.

- The structures associated with the flats are often interpreted as the result of shortening, but as mentioned in nature (e.g. Sharp et al., 2000; Jackson and Rotevatn, 2013) and shown by the experiment here (e.g. Horsfield, 1977), it is possible to create both a forced fold and reverse fault in pure extension when the stratigraphy is not homogeneous, but is instead comprised of an alternation between brittle and ductile layers. Therefore, it is very important to characterise these typical structures in order to avoid misinterpretation.

Acknowledgements

We acknowledge Total for financial support (contract number: FR 00005432). Special thanks are given to J.-J. Kermarrec for his valuable technical assistance and availability, as always. We thank Sara Mullin for post-editing the English style. We are grateful to Antonio Casas and Tim Dooley for their constructive review, comments and suggestions that helped us improve our manuscript.

References

Allemand, P., Brun, J.-P., Davy, P., Van Den Driessche, J., 1989. Symétrie et asymétrie des rifts et mécanismes d'amincissement de la lithosphère. Bull. la Société Géologique Fr. 3, 445–451.

Ballard, J.F., Brun, J.P., Van Den Driessche, J., Allemand, P., 1987. Propagation des chevauchements au-dessus des zones de décollement: Modèles expérimentaux. Comp. Rend. Académie Sci. Paris Sér. IIA 305, 1249–1253.

Balé, P., 1986. Tectonique cadomienne en Bretagne nord. Interaction décrochement chevauchement: champs de déformation et modélisations expérimentales. Ph.D. thesis. Université de Rennes 1.

Brun, J.-P., Nalpas, T., 1996. Graben inversion in nature and experiments. Tectonics, 15 (2) 677–687.

Caumon, G., Collon-Drouaillet, P., Le Carlier de Veslud, C., Viseur, S., Sausse, J., 2009. Surface-Based 3D Modeling of Geological Structures. Math. Geosci. 41, 927–945. doi:10.1007/s11004-009-9244-2.

Childs, C., Manzocchi, T., Walsh, J. J., Bonson, C. G., Nicol, A., Schöpfer, M. P., 2009. A geometric model of fault zone and fault rock thickness variations. Journal of Structural Geology 31(2), 117–127.

Cohen, H.A., McClay, K.R., 1996. Sedimentation and shale tectonics of the northwestern Niger Delta front. Mar. Petrol. Geol. 13, 313–328.

Cosgrove, J.W., Ameen, M.S. (Eds.), Forced folds and fractures. Geol. Soc. Lond. Spec. Publ. 169, 225p.

Dauteuil, O., Bourgeois, O., Mauduit, T., 2002. Lithosphere strength controls oceanic transform zone structure: insights from analogue models. Geophysical Journal International, 150(3), 706–714.

Davy, P., Cobbold, P.R., 1991. Experiments on shortening of a 4-layer model of continental lithosphere. Tectonophysics 188, 1–25.

Davy, P., Hansen, A., Bonnet, E., Zhang, S. Z., 1995. Localization and fault growth in layered brittle-ductile systems: Implications for deformations of the continental lithosphere. Journal of Geophysical Research: Solid Earth, 100(B4), 6281–6294.

Dooley, T., McClay, K.R., Pascoe, R., 2003. 3D analogue models of variable displacement extensional faults: applications to the Revfallet fault systems, Mid-Norway, in Nieuland, D. A., ed., New insights into structural interpretation and modelling: Geological Society of London, Special Publication 212, 151–167.

Du Bernard, X., 2002. Les modes de la localisation et de propagation de la rupture dans les zones de failles affectant les grès, et les facteurs qui les contrôlent. Ph.D. thesis. Université Joseph-Fourier - Grenoble I.

Faugère, E., Brun, J.-P., 1984. Modélisation expérimentale de la distension continentale. Comp.-Rend. Académie Sci. 299, 365–370.

Fossen, H., Rotevatn, A., 2016. Fault linkage and relay structures in extensional settings—A review. Earth-Science Reviews 154, 14–28.

Ge, H., Jackson, M.P.A., 1998. Physical modeling of structures formed by salt withdrawal; implications for deformation caused by salt dissolution. AAPG Bull. 82, 228–250.

449 Hardy, S., McClay, K., 1999. Kinematic modelling of extensional fault-propagation folding. J.
450 Struct. Geol. 21, 695–702.
451 Higgins, R.I., Harris, L.B., 1997. The effect of cover composition on extensional faulting above re-
452 activated basement faults: results from analogue modelling. J. Struct. Geol. 19, 89–98.
453 doi:10.1016/S0191-8141(96)00083-1.
454 Horsfield, W. T. "An experimental approach to basement-controlled faulting."Geologie en
455 Mijnbouw 56.4 (1977): 363–370.
456 Jackson, C.A.L., Rotevatn, A., 2013. 3D seismic analysis of the structure and evolution of a salt-
457 influenced normal fault zone: a test of competing fault growth models. J. Struct. Geol. 53.
458 http://dx.doi.org/10.1016/j.jsg.2013.06.012.
459 Kristensen, M. B., Childs, C. J., Korstgård, J. A., 2008. The 3D geometry of small-scale relay zones
460 between normal faults in soft sediments. Journal of Structural Geology, 30(2), 257–272.
461 Lacoste, A., Vendeville, B. C., Mourgues, R., Loncke, L., Lebacq, M., 2012. Gravitational
462 instabilities triggered by fluid overpressure and downslope incision–Insights from analytical
463 and analogue modelling. Journal of Structural Geology, 42, 151–162.
464 Le Carlier de Veslud, C., Cuney, M., Lorilleux, G., Royer, J.J., Jébrak, M., Kister, P., 2009. 3D
465 modeling of uranium-bearing solution-collapse breccias in Proterozoic sandstones (Athabasca
466 Basin, Canada). Computer and Geosciences 2, 92–107.
467 Lewis, M.M., Jackson, C.A.-L., Gawthorpe, R.L., 2013. Salt-influenced normal fault growth and
468 forced folding: The Stavanger Fault System, North Sea. J. Struct. Geol. 54, 156–173.
469 doi:10.1016/j.jsg.2013.07.015.
470 Malavieille, J., 1984. Modélisation expérimentale des chevauchements imbriqués: application aux
471 chaînes de montagnes. Bull. Société Géologique Fr. 26, 129–138.
472 Mallet, J.L., 2002. Geomodeling. Applied Geostatistics. Oxford University Press, New York.

McClay, K.R., 1990. Extensional fault systems in sedimentary basins: a review of analogue model studies. Mar. Pet. Geol. 7, 206–233.

McClay, K.R., Scott, A.D., 1991. Experimental models of hangingwall deformation in ramp-flat listric extensional fault systems. Tectonophysics 188, 85–96.

Mourgues, R., Cobbold, P.R., 2003. Some tectonic consequences of fluid overpressures and seepage forces as demonstrated by sandbox modelling. Tectonophysics 376, 75–97.

Nalpas, T., Le Douaran, S., Brun, J.-P., Unternehr, P., Richert, J.-P., 1995. Inversion of the Broad Fourteens Basin (Offshore Netherlands). A small-scale model investigation. Sediment. Geol., 95, 237–250.

Nalpas, T., Brun, J.P. 1993. Salt flow and diapirism related to extension at crustal scale: Tectonophysics 228, 349–362.

Panien, M., Schreurs, G., Pfiffner, A., 2006. Mechanical behaviour of granular materials used in analogue modelling: insights from grain characterisation, ring-shear tests and analogue experiments. J. Struct. Geol. 28, 1710–1724. doi:10.1016/j.jsg.2006.05.004.

Peacock, D.C.P., Sanderson, D.J., 1991. Displacements, segment linkage and relay ramps in normal fault zones. J. Struct. Geol. 13, 721–733.

Richardson, N.J., Underhill, J.R., Lewis, G., 2005. The role of evaporite mobility in modifying subsidence patterns during normal fault growth and linkage, Halten Terrace, Mid-Norway. Basin Res. 17, 203–223. doi:10.1111/j.1365-2117.2005.00250.x.

Rykkelid, E., Fossen, H., 2002. Layer rotation around vertical fault overlap zones: observations from seismic data, field examples, and physical experiments. Marine and Petroleum Geology, 19(2), 181–192.

Schlische, R.W., 1995. Geometry and origin of fault-related folds in extensional settings. AAPG Bull. 79, 1661–1678.

Sharp, I.R., Gawthorpe, R.L., Underhill, J.R., Gupta, S., 2000. Fault-propagation folding in extensional settings: Examples of structural style and synrift sedimentary response from the Suez rift, Sinai, Egypt. Geol. Soc. Am. Bull. 112, 1877–1899.

Stewart, S.A., Harvey, M.J., Otto, S.C., Weston, P.J., 1996. Influence of salt on fault geometry: examples from the UK salt basins. Geol. Soc. Lond. Spec. Publ. 100, 175–202. doi:10.1144/GSL.SP.1996.100.01.12.

Soto, R., Casas-Sainz, A.M., Del Río, P., 2007. Geometry of half-grabens containing a mid-level viscous décollement. Basin Research 19 (3), 437–450. doi: 10.1111/j.1365-2117.2007.00328.

Vendeville, B., 1987. Champs de failles et tectonique en extension : modélisation experimentale. Mém. Doc. Cent. Armoricain. Etud. Struct. Socles., 15, Rennes.

Weijermars, R., Jackson, M.P.A., Vendeville, B., 1993. Rheological and tectonic modeling of salt provinces. Tectonophysics 217, 143–174.

Withjack, M.O., Olson, J., Peterson, E., 1990. Experimental models of extensional forced folds (1). AAPG Bull. 74, 1038–1054.

Withjack, M.O., Callaway, S., 2000. Active normal faulting beneath a salt layer: an experimental study of deformation patterns in the cover sequence. AAPG Bull. 84, 627–651.

Wu, J.E., McClay, K., 2011. Two-dimensional Analog Modeling of Fold and Thrust Belts: Dynamic Interactions with Syncontractional Sedimentation and Erosion. In: McClay, K., Shaw, J., Suppe, J. (Eds.), Thrust fault-related folding. American Association of Petroleum Geologists Memoir 94, pp. 301–333. http://dx.doi.org/10.1306/13251343M9450.

Figure captions

Figure 1: Multi-scale examples showing a normal fault geometry in a brittle-ductile system, the bleu line show a fold associated to a flat of the fault (in red): a1) thin section and a2) corresponding line drawing from La Moutiere (Southern Alps, France) where the (-) symbol indicates a very fined-grained lithology and (+) symbols indicate a coarser-grained layer (modified from Du Bernard, 2002); b) outcrop photograph with alternating layers of chalk and marl at Flamborough (Yorkshire, UK, modified from Childs et al., 2009); c) seismic section and line drawing from the Gulf of Suez (modified from Jackson and Rotevatn, 2013); d) seismic profile and line drawing from the Stavanger Fault System (North Sea, modified from Lewis et al., 2013); e) analogue modelling of an extensional forced-fold associated with a precut flat-ramp fault (Expt. E59-2, modified from McClay, 1990).

Figure 2: Experimental apparatus and strength profile on left side.

Figure 3: Schematic cross-section showing the main structural features of the experiments (standard stratigraphy, experiment 3). Zoom with a forced fold related to the fault flat geometry at left.

Figure 4: Cross-sections showing the effect of displacement rate on the final deformation (amount of extension: 1 cm in all experiments).

Figure 5: a) Global view of the 3D numerical model (of experiment 3) with a top view photograph applied onto the topography; b) 3D fault network showing that the deformation is heterogeneous and varied. Orange surfaces are normal faults, green surfaces reverse faults and blue surfaces the flats.

Figure 6: Cross-sections showing the effect of the amount of extension on the final deformation (extension velocity: 1 cm/h in all experiments).

Figure 7: Cross-sections showing the influence of ductile thickness and the location of the ductile layers on the final deformation.

544 Figure 8: Diagram showing the different types of structures in relation to vertical movements in a

545 extensional context.

546 Table 1: Experimental parameters.

name	extension rate (cm/h)	extension (cm)	silicone thickness (cm)	layer order from base to top (where flat may be created)
1 (FANEX 3)	**0.25**	**1**	**0.5**	**microbeads/pink silicone /transparent silicone**
2 (FANEX 2)	**0.5**	**1**	**0.5**	**microbeads/pink silicone /transparent silicone**
3 (FANEX 4)	**1**	**1**	**0.5**	**microbeads/pink silicone /transparent silicone**
4 (FANEX 5)	**2**	**1**	**0.5**	**microbeads/pink silicone /transparent silicone**
5 (FANEX 16)	**4**	**1**	**0.5**	**microbeads/pink silicone /transparent silicone**
6 (FANEX 8)	**1**	**0.5**	**0.5**	**microbeads/pink silicone /transparent silicone**
7 (FANEX 1)	**1**	**2**	**0.5**	**microbeads/pink silicone /transparent silicone**
8 (FANEX 17)	**1**	**4**	**0.5**	**microbeads/pink silicone /transparent silicone**
9 (FANEX 7)	**1**	**1**	**0.25**	**microbeads/pink silicone /transparent silicone**
10 (FANEX 6)	**1**	**1**	**0.5**	**transparent silicone /pink silicone / microbeads**

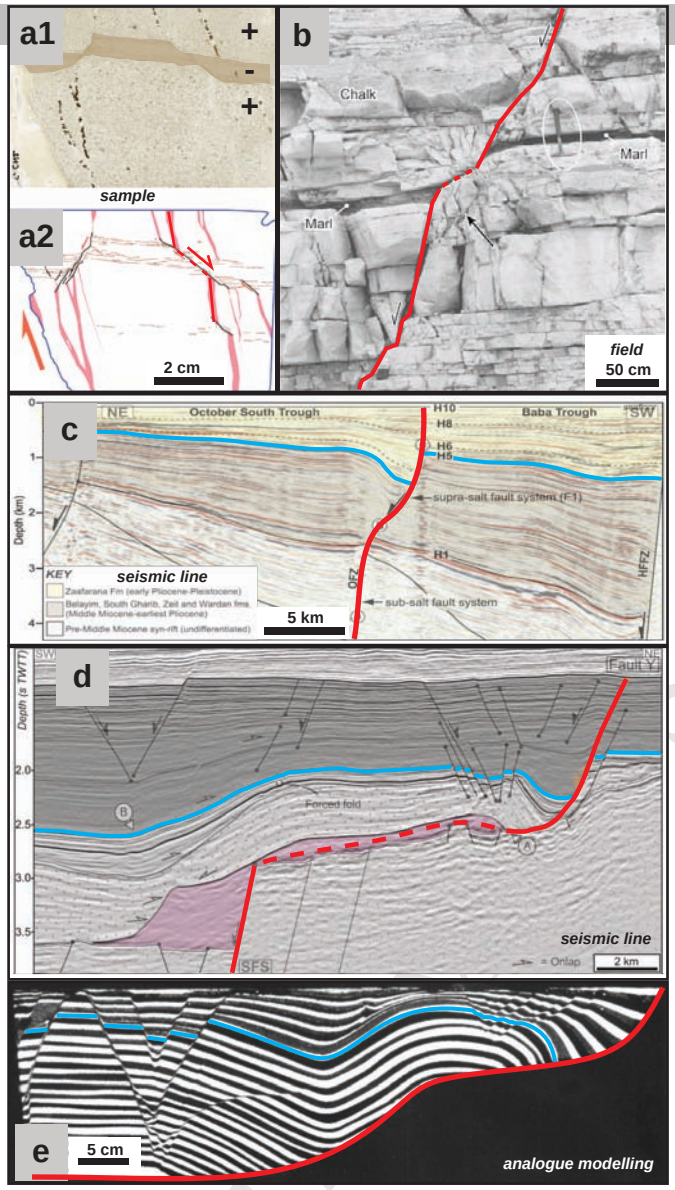

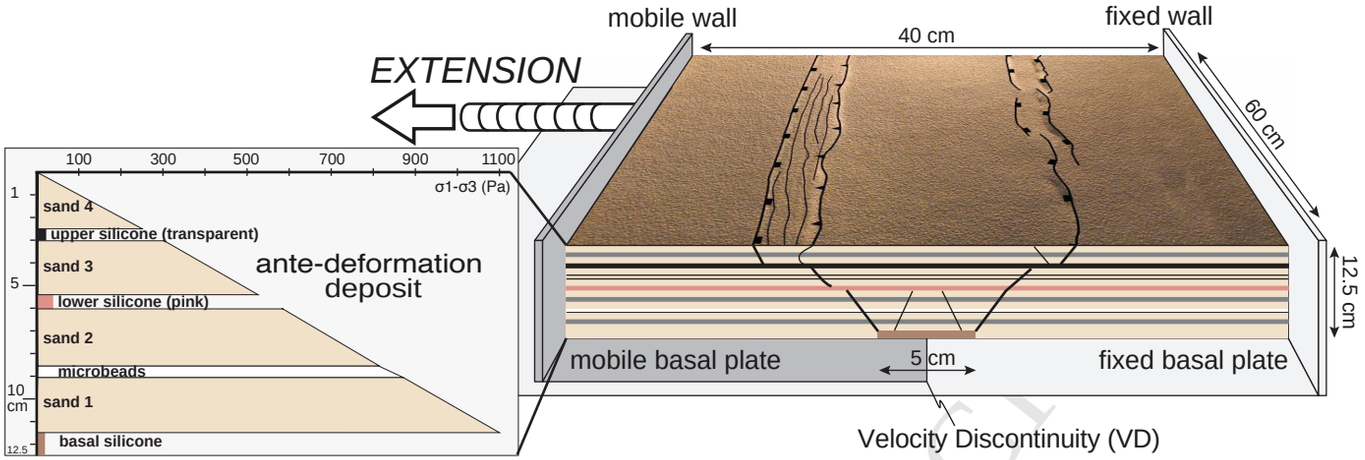

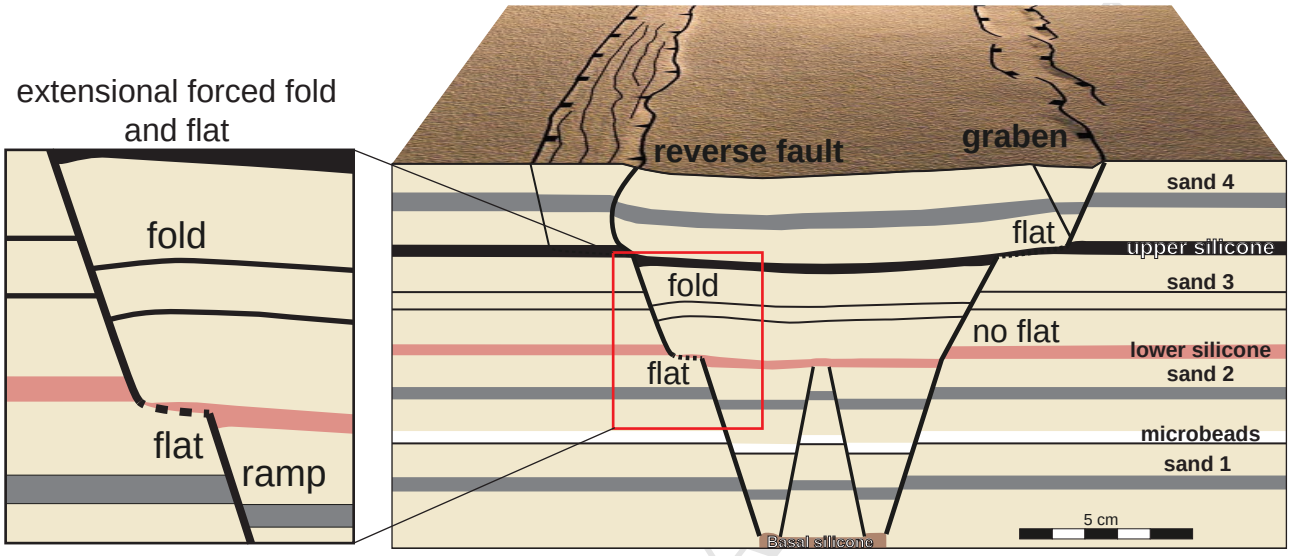

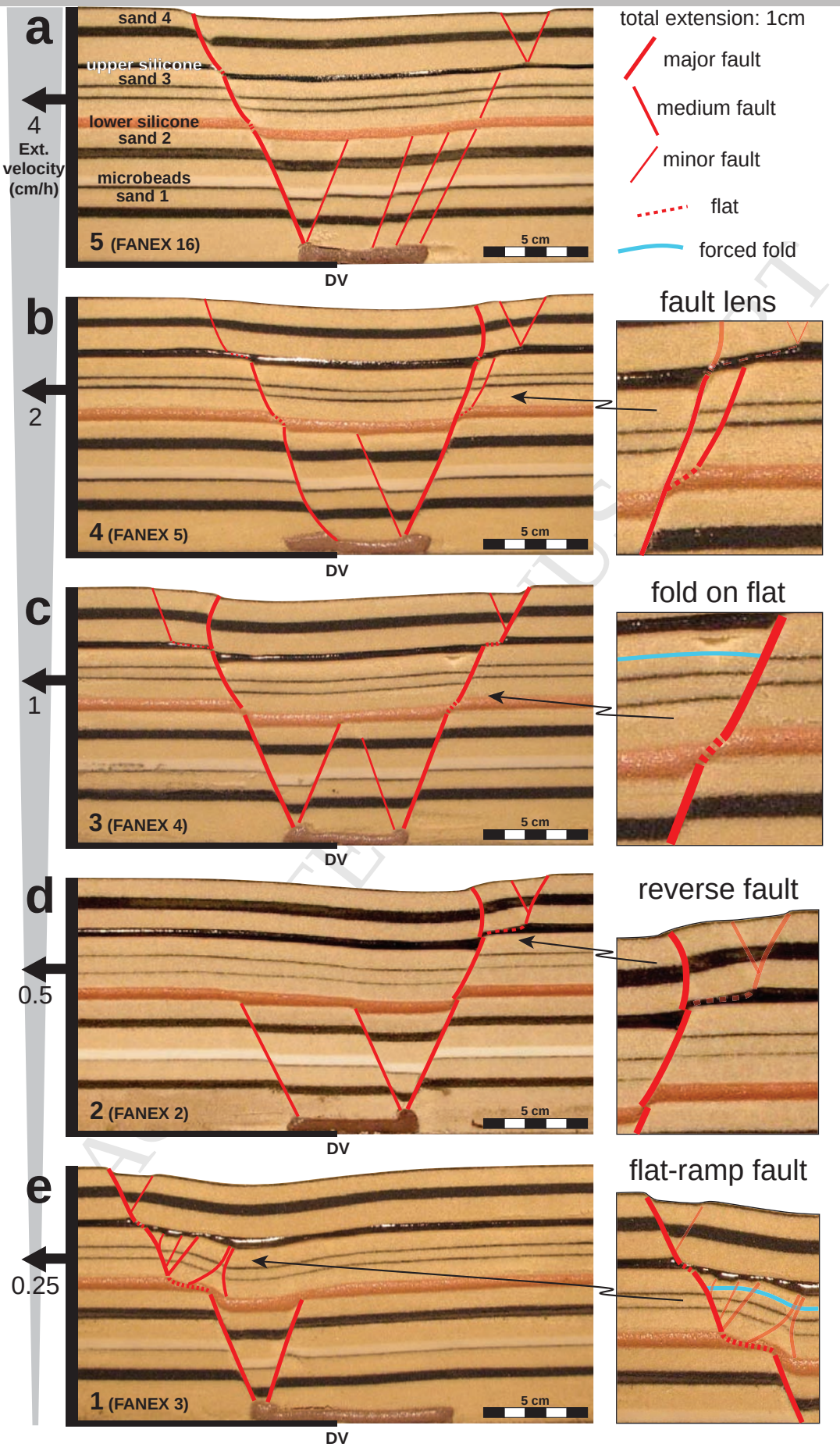

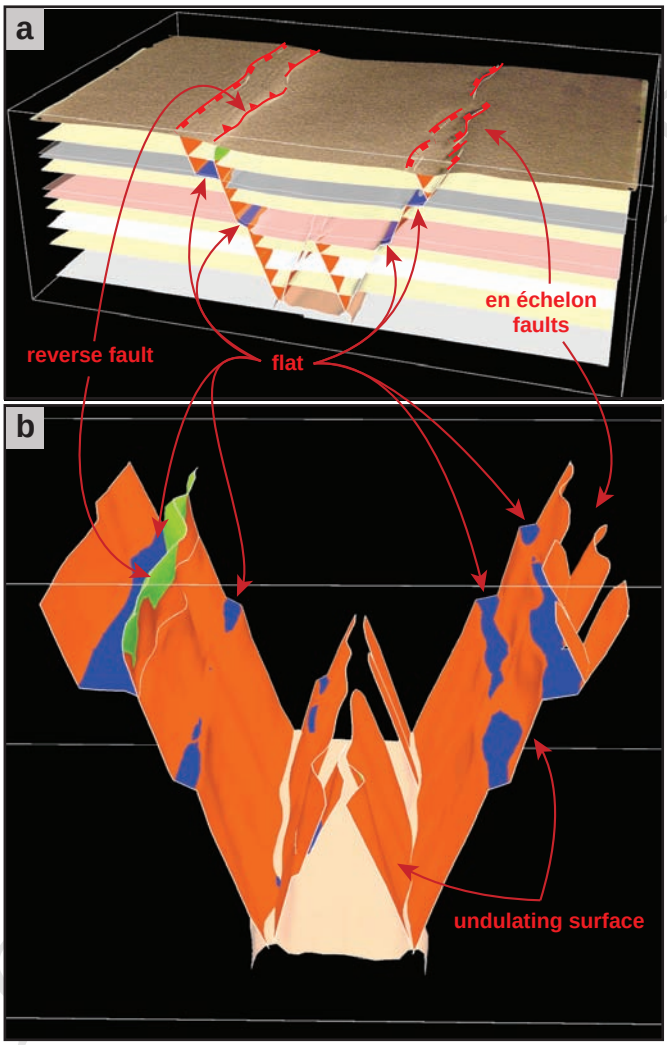

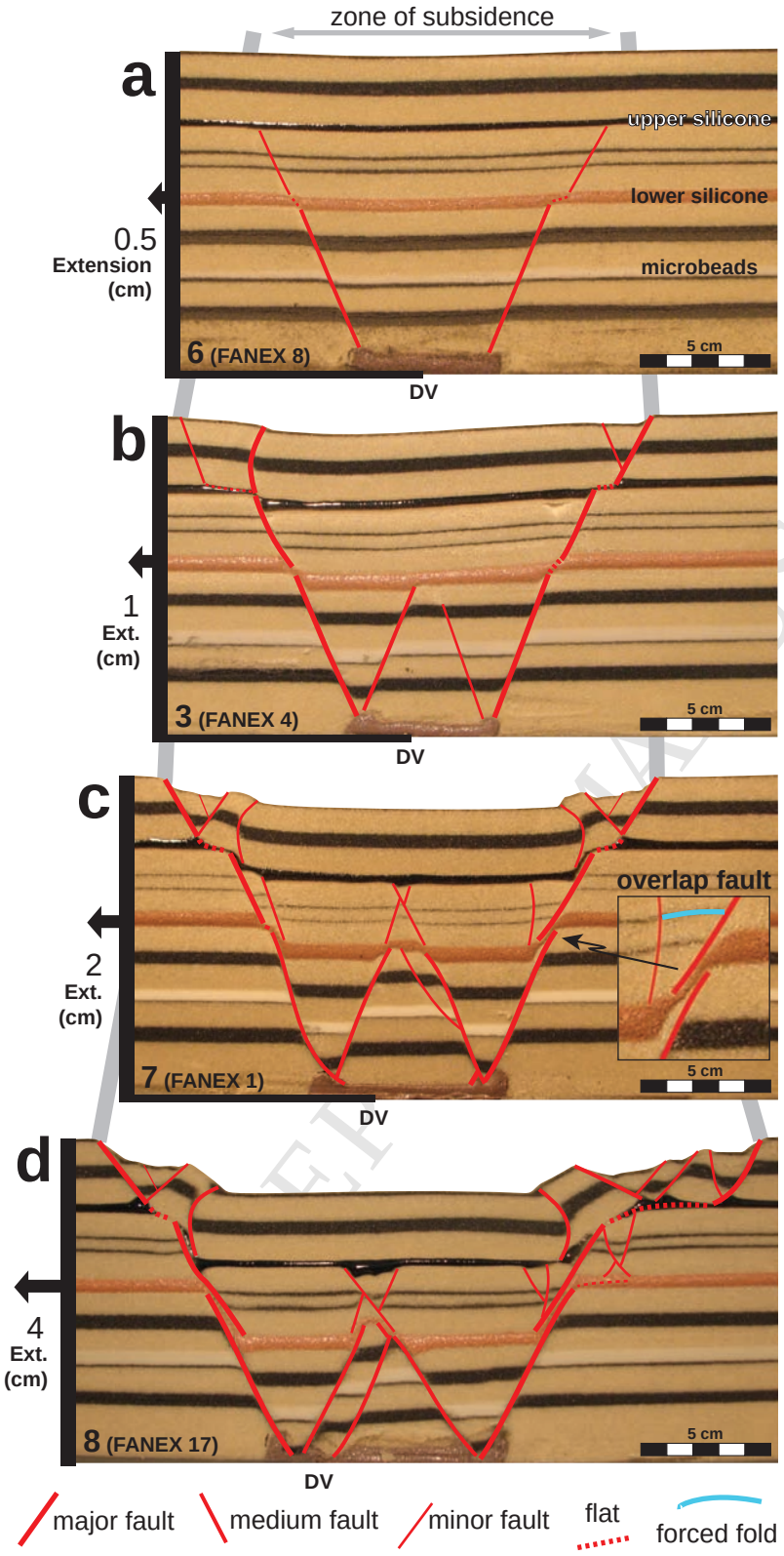
zone of subsidence
a
upper silicone
lower silicone
microbeads
0.5
Extension
(cm)
6 (FANEX 8)
5 cm
DV
b
1
Ext.
(cm)
3 (FANEX 4)
5 cm
DV
c
overlap fault
2
Ext.
(cm)
7 (FANEX 1)
5 cm
DV
d
4
Ext.
(cm)
8 (FANEX 17)
5 cm
DV
major fault
medium fault
minor fault
flat
forced fold

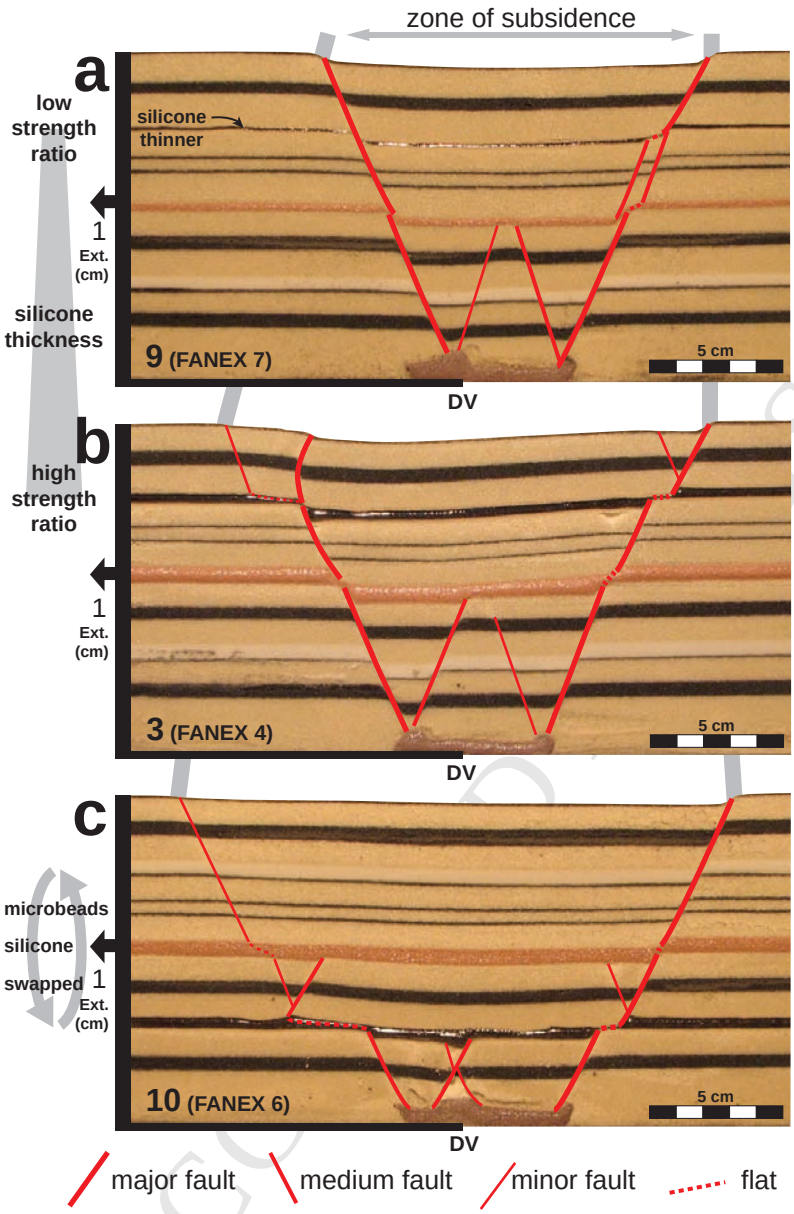
zone of subsidence
a
low strength ratio
silicone thinner
1 Ext. (cm)
silicone thickness
9 (FANEX 7)
5 cm
DV
b
high strength ratio
1 Ext. (cm)
3 (FANEX 4)
5 cm
DV
c
microbeads
silicone
swapped
1 Ext. (cm)
10 (FANEX 6)
5 cm
DV
major fault
medium fault
minor fault
flat

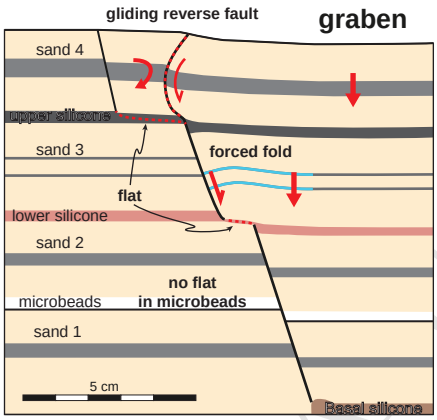

www.cnrs.fr
UMR CNRS 6118
www.geosciences.univ-rennes1
http://osur.univ-rennes1.fr
www.univ-rennes1.fr

Rennes 26/06/2017

Thierry NALPAS
Maître de conférences

Reference: Vasquez et al, Highlights

The main point of the presented manuscript are:
- The control of the geometry of normal faults related to the presence of décollement levels;
- The geneses of flats along normal faults;
- The geneses of forced fold in the hanging wall of a normal fault;
- The geneses of gliding reverse faults in the hanging wall of a normal fault.

It is very important to recognize that these structures may be generated in a pure extensional system, and to not associate them systematically with compression, strike-slip movement or inversion.